Analytical Modelling of Magnetic DW Motion

Physics Procedia

Volume 75, 2015, Pages 974–985

20th International Conference on Magnetism

Analytical Modelling of Magnetic DW Motion

S. Ali Nasseri[1,2], Bhaskarjyoti Sarma[1,2], Gianfranco Durin[1,3], and Claudio Serpico[1,4]

[1] ISI Foundation, Via Alassio 11/c, 10126 Torino, Italy
[2] Politecnico di Torino, Corso Duca degli Abruzzi 24, 10129 Torino, Italy
[3] Istituto Nazionale di Ricerca Metrologica (INRIM), Strada delle Cacce 91, 10135 Torino, Italy
[4] Università degli Studi di Napoli Federico II, Via Claudio 21, 80125 Napoli, Italy

Abstract

The main analytical model for describing the motion of magnetic domain walls is the 1-D model formulated based on the profile of a Bloch wall. This model qualitatively describes the motion of magnetic domain wall in nanowires, while it may fail to match experimental and numerical results quantitatively. In recent years, the 1-D model has been further generalized by the introduction of terms such as spin transfer torques and spin orbit torques. It has also been used to describe the motion of different domain walls, including vortex walls. It seems that in many such attempts, formalisms are not followed accurately and the main assumptions of the model (such as the Bloch wall profile used in developing the model) are underestimated. In this paper, we first derive an analytical model to describe the motion of a tilting Bloch wall in perpendicularly magnetized materials using four collective coordinates. We then compare the energy landscape predicted by this model to that of micromagnetic simulations, highlighting the possibility of using such comparisons to develop corrections for the 1-D model.

Keywords: Magnetic domain wall motion, 1-D model, Analytical modeling of magnetic DW motion, collectove coordinates approach

1 Introduction

One of the promising fields of technological advancement is the area of spintronics, in which both charge and spin degrees of freedom of electrons are exploited to design devices with improved performance, and power consumption at lower cost [1, 2]. Fuelled by the limitations of current technologies in improving the performance of devices such as storage media, scientists have focused on developing a fundamental understanding of spintronic phenomena and proposing possible applications for these new discoveries [3, 4, 5, 6, 7].

Advances in manufacturing have led to the miniaturization of electronic components towards nanoscale devices. Manipulating magnetic domain walls (DWs) within nanostructures has been linked with applications in the development of spintronic logic [8, 9, 10], storage [11, 12, 13] and sensing [14] devices. Such applications have led to increased interest within the scientific

Selection and peer-review under responsibility of the Scientific Programme Committee of ICM 2015

doi:10.1016/j.phpro.2015.12.133

community in developing models which can qualitatively or quantitatively describe magnetic domain wall motion under applied fields and currents.

In this work, after a brief review of magnetization dynamics, a one-dimensional model is developed to describe the dynamics of a tilted Bloch wall in multilayer nanowires. Energy predictions from this model for a case of field-driven DW motion are then compared with micromagnetic simulations in order to assess possible approaches to improving the accuracy of the analytical model.

2 Magnetization Dynamics: A Phenomenological Approach

The Landau-Lifshitz-Gilbert equation is a phenomenological relationship used to describe magnetization dynamics:

$$\frac{d\vec{m}}{dt} = -\gamma\vec{m} \times \vec{H}_{eff} + \alpha\vec{m} \times \frac{d\vec{m}}{dt} \tag{1}$$

in which γ is the gyromagnetic ratio, $\vec{m}$ is the normalized magnetization vector, $\vec{H}_{eff}$ is the effective magnetic field acting on the magnetization and α is the phenomenological Gilbert damping, formulated based on the Lagrangian approach [15]. The LLG equation constitutes two torques: a torque by the effective field trying to precess the magnetization, and a damping torque perpendicular to the former.

The effective field in the LLG equation is key to understanding magnetization dynamics. This field includes internal interactions within the magnetic material and may include external stimulation of the system due to fields, currents and interfacial effects. The effective field is related to the energy of the different interactions through $\vec{H}_{eff} = \frac{\delta E}{\delta \vec{m}}$. The major energy terms inherent to a ferromagnetic sample include exchange, magnetic anisotropy, and magnetostatic energies. Any applied external field will also contribute to the effective field through an associated Zeeman energy term. In the presence of an applied field, the total energy may be written as:

$$E = \overbrace{A\sum_{i=1}^{3}|\nabla m_i|^2}^{Exchange} + \overbrace{sin^2\theta(K_0 + K_1 sin^2\phi)}^{Anisotropy} - \overbrace{\mu_0 M_s \vec{H}_a \cdot \vec{m}}^{Zeeman} \tag{2}$$

In the above formulation, the magneostatic energy is included as shape anisotropy in the anisotropy energy term with the constant K_1, a formulation which is valid for nanowire geometries.

When a current is injected in a ferromagnetic material, it gives rise to spin transfer torques (STTs) which can move a DW in this material [16, 17]. Two underlying mechanisms contribute to DW motion through STT: Linear momentum transfer and electron reflection, and adiabatic electron transmission.

These two processes can be modelled by adding two terms in the LLG equation: An adiabatic term taking into account the ideal case of full spin reflection and a non-adiabatic term which stems from spin relaxation and non-adiabatic effects during transmission. The torques on the magnetization due to these terms may be written as [18, 19]:

$$\tau_{STT} = \overbrace{-(\vec{u}\cdot\nabla)\vec{m}}^{adiabatic} + \overbrace{\beta\vec{m} \times ((\vec{u}\cdot\nabla)\vec{m})}^{non-adiabatic} \tag{3}$$

in which β is the nonadiabaticity coefficient and $\vec{u} = \frac{\vec{J}Pg\mu_b}{2eM_s}$, with J denoting current density and P denoting the polarization rate of the current. The adiabatic torque is also known as the in-plane or Slonczewski-like torque (the torque being in the same direction as the damping torque), while the non-adiabatic term is also called the field-like torque, perpendicular torque or β term (the torque being in the same direction as the torque due to the effective field). The direction of DW motion in STT is the same as that of electron motion or opposite current flow. Note that the non-adiabatic torque is the driving force in DW motion, while the adiabatic torque competes with damping. As is evident from the above models, in STT the magnetization of each magnetic moment is coupled with that of other moments in the sample at other positions.

In recent years, DW studies have focused on complex heterostructures. In these structures, interfacial effects also contribute to DW motion. Current dependant spin-orbit interactions are observed in systems with a ferromagnetic layer sandwiched between two heavy metal layers or a heavy metal layer and an oxide layer. Such effects stem from the fact that the flow of electric current in a crystalline structure lacking inversion symmetry can transfer orbital angular momentum from the lattice to the spins, giving rise to effects which can enhance the STT or act on their own to move DWs.

Current dependant spin-orbit interactions include the Spin Hall Effect (SHE) and the Rashba effect. In SHE, spin dependant scattering in the heavy metal layer leads to spin accumulation at lateral boundaries with opposite spins accumulating on opposite boundaries [20]. This leads to a spin current perpendicular to the charge current and interface normal. The Rashba effect becomes important when the ferromagnetic layer is sandwiched between two dissimilar layers (a heavy metal layer and an oxide layer for example). Simultaneous magnetization, spin orbit interactions and broken inversion symmetry at the interface altogether lead to this effect. An electric field is created between the sandwiching layers which affects spins in the ferromagnetic layer.

The main torques stemming from these two effects may be modelled as [21]:

$$\tau_{SOT} = \overbrace{\gamma\tau_{FL}(\vec{m} \times \hat{u}_{SOT})}^{field-like} - \overbrace{\gamma\tau_{SL}\vec{m} \times (\vec{m} \times \hat{u}_{SOT})}^{Slonczewski-like} \tag{4}$$

in which $\hat{u}_{SOT} = \hat{J} \times \hat{n}$ is the direction of spin current when $\hat{j}$ is the direction of current flow in the heavy metal layer and $\hat{n}$ is the interface normal. These two torques are called the homogeneous torques, as higher order torques are not included in the above formulation [22, 23]. While both the SHE and Rashba effects contribute to these torques, it has been suggested [21] that, effectively $\tau_{FL}^{SHE} << \tau_{SL}^{SHE} = \frac{\hbar\Phi_h J}{2eM_s t}$ in which Φ_h is the spin-hall angle which signifies the strength of the spin-hall effect and t is the layer thickness. It has also been suggested that $\tau_{SL}^{Rashba} << \tau_{FL}^{Rashba} = \frac{\alpha_R JP}{\mu_B M_s}$ in which α_R is a parameter outlining the strength of the Rashba effect.

An example of current independent spin-orbit interactions is the interfacial Dzyaloshinski-Moriya Interaction (DMI) which stems from interfacial spin-orbit coupling. This effect may be included in the effective field as:

$$H_{DMI} = -\vec{D} \cdot (\vec{S_1} \times \vec{S_2}) \tag{5}$$

where $\vec{D}$ is the DMI vector. The energy associated with the DMI for a sample isotropic in the plane, where the Dzyaloshinskii vector originated from symmetry breaking at the z surface, may be calculated as [24]:

$$E_{DMI} = D(m_z \nabla.\vec{m} - (\vec{m}.\nabla)m_z) \tag{6}$$

where D is a uniform constant signifying the strength of the DMI interaction.

Other effects may also be included in the LLG equation. For example, pinning is usually modelled using a quadratic [25] or harmonic[26] pinning potential added to the energy landscape of the system. Thermal effects and wire roughness may also be included as stochastic processes changing the energy landscape of the system [27, 28]. Finally, the effect of defects may be included using a non-linear dry friction dissipation model [29]. We will not include such effects in this work.

3 Towards an Analytical Model

As previously mentioned, the LLG equation could be used to describe magnetization dynamics in a ferromagnetic system. Yet, solving this equation requires quantification of magnetization in Cartesian or spherical coordinates and discretization of the solution domain to solve the equations, which can be time consuming and computationally costly.

Our aim is to change the coordinates used in the model to more collective physical coordinates relating to the DW and to also reduce the number of degrees of freedom being studied so the equations may be solved analytically. For such an approach, it seems reasonable to develop a Lagrangian description of magnetization dynamics, so coordinate changes could be properly applied. The Euler-Lagrange formulation has the added benefit of being capable of incorporating dissipative functions, which stem from damping and Slonczewski-like torques.

Our aim is to solve the inverse problem of finding the Lagrangian and Rayleigh dissipation function that can regenerate the LLG equation if put in the Euler-Lagrange-Rayleigh equation:

$$\frac{\partial L}{\partial q_i} - \frac{d}{dt}\left(\frac{\partial L}{\partial \dot{q}_i}\right) + \frac{\partial F}{\partial \dot{q}_i} = 0 \tag{7}$$

In this case, it seems simpler to use a set of spherical coordinates to describe magnetization. We are interested in magnetic DW dynamics in a perpendicularly magnetized system made of a heterostructure of a heavy metal layer, a ferromagnetic layer and another heavy metal layer (or alternatively an oxide layer). The spherical coordinates selected for this problem are depicted in Figure 1.a. The normalized magnetization vector in this case (assuming a constant saturation magnetization, M_s) is:

$$\vec{m} = (sin\theta cos\psi, sin\theta sin\psi, cos\theta) \tag{8}$$

This helps in describing magnetization as a spinning top, aiding in the development of the Lagrangian. Note that, while the coordinates θ and ψ are useful for calculations, they do not posses physical meaning to collectively describe the dynamics of the DW.

It can be shown that the following Lagrangian density and dissipation density functions can be used in the Euler-Lagrange equation to derive the LLG [30]:

$$\frac{d^3L}{dr^3} = l = E + E_{DMI} + \overbrace{\frac{M_s}{\gamma}\dot{\psi}cos\theta}^{PrecessionTerm} \overbrace{-\frac{uM_s}{\gamma}\psi\frac{d(cos\theta)}{dx}}^{STT} \overbrace{-\mu_0 M_s \tau_{FL}\vec{m}\cdot\hat{u}_{SOT}}^{SOT} \tag{9}$$

$$\frac{d^3F}{dr^3} = f = \frac{\alpha M_s}{2\gamma}\left[\frac{d\vec{m}}{dt} + \frac{\beta}{\alpha}(\vec{u}\cdot\nabla)\vec{m} - \frac{\mu_0\gamma\tau_{SL}}{\alpha}\vec{m}\times\vec{u}_{SOT}\right]^2 \tag{10}$$

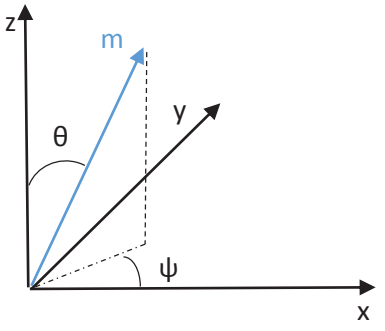

(a) Spherical coordinates used in this paper.

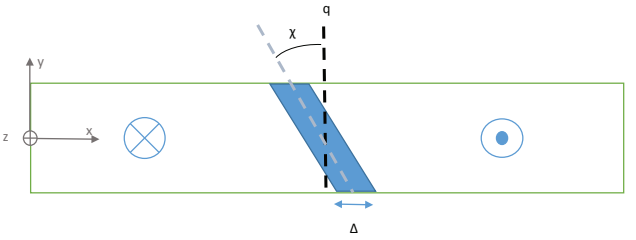

(b) Collective coordinates (ϕ not shown).

(c) t=0, D=1 mJ/m^2

(d) t=100ps, D=1 mJ/m^2

(e) t=0, D=2 mJ/m^2

(f) t=100ps, D=2 mJ/m^2

Figure 1: The selected collective coordinates and snapshots from micromagnetic simulations with an applied field of 10mT. (d) and (e) clearly show the tilting of the DW, when compared to the initial DWs illustrated in (c) and (f) respectively. Note that (e) also shows the partial deformation of the DW at high fields.

4 A Collective Coordinates Approach to Magnetic DW Motion

The Lagrangian developed above, while not unique, can be used to derive the LLG equation from the Euler-Lagrange equation. However, our aim is to develop a collective description of DW motion; a description which does not rely on the properties of each single magnetic moment in the system, but directly describes the motion of the DW as the entity being studied. To do so we need to introduce assumptions in order to connect the spatial change of magnetization with the coordinates of interest.

The system of interest in this paper is a multilayer perpendicularly magnetized nanostrip containing a magnetic DW. To describe DW motion in this system, the following collective coordinates were selected:

1. The position of the centre of the DW (q);
2. The tilt angle of the magnetization out of the plane of the DW (ϕ);
3. The domain wall width (Δ);
4. The tilt angle of the wall in the plane of the sample (χ) .

The coordinates above are depicted in Figure 1.b. They were selected based on previous work on this topic [31, 32, 30]; this is the first attempt to include all four coordinates together to describe DW motion. Note that all these four coordinates are time dependent. The coordinate χ was included in order to model the effects of the DMI, which tends to tilt the DW, as depicted in Figure 1.d and f.

In order to move from a description based on spherical coordinates to collective coordinates, the two coordinate systems need to be linked. To relate the two coordinate systems, we may use the profile of a semi-elastic tilted Bloch or Néel wall as an ansatz:

$$\theta = 2arctan\left[exp\left(\frac{(x-q)cos\chi + ysin\chi}{\Delta}\right)\right] \tag{11}$$

along with $\psi(x, y, t) = \phi(t)$.

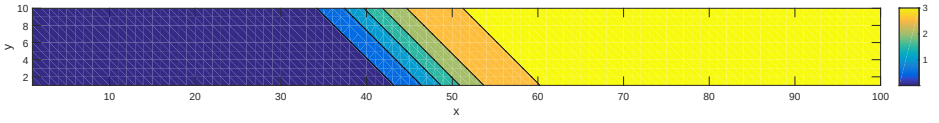

(a) Variation of θ with x and y for $\Delta = 3$ and $\chi = 45$ deg. The DW tilting angle can clearly be seen in this figure.

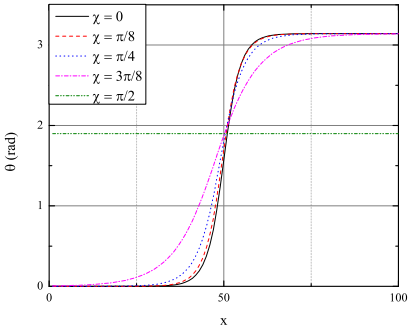

(b) Variation of θ with the DW tilt angle (χ) for $\Delta = 3$ and $y = 0$.

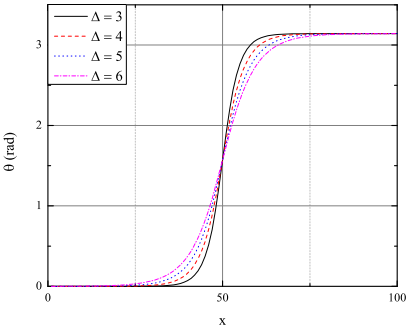

(c) Variation of θ with DW width (Δ) for $\chi = 45$ deg and $y = 0$.

Figure 2: Variation of the θ calculated from the ansatz with different parameters. (a) clearly shows that the wall is tilting as we traverse the width of the material. (b) shows the effect of changing χ and (c) highlights that changing Δ changes the width of the wall. It is clear that the ansatz becomes invalid at high values of χ.

The ansatz above (Eq. 11) is a generalization of the original ansatz used by Slonczewski [31] with the additional parameter χ added to account for the tilting of the wall and the DW

width Δ included as a time dependant coordinate. The range for θ using this function is [0,π], matching the magnetization behaviour in real systems. Figure 2 highlights the effect of changing the ansatz parameters. It is evident that for large values of χ, the ansatz becomes invalid and it no longer describes the right magnetization profile. Also note that the ansatz is not valid for high values of DMI, as clear by the different tilting behaviour at high DMI strength in Figure 1.f.

The introduction of this ansatz links the spherical coordinates to our collective coordinates. Yet, at the same time this means that the motion of the system is now constrained due to the ansatz; the motion no longer follows the exact LLG equation, but a form of the LLG with additional torques which constrain the dynamics of the magnetic moments so that the requirements of the ansatz are met. These constraints could also explain why micromagnetic simulations do not exactly match 1-D model predictions in some cases (for examples see references [30, 33]).

The ansatz has the following properties which simplify integration of the Lagrangian and dissipation density functions:

$$\frac{\partial\theta}{\partial x} = \frac{cos\chi}{\Delta} sin\theta \tag{12}$$

$$\frac{\partial\theta}{\partial y} = \frac{sin\chi}{\Delta} sin\theta \tag{13}$$

$$\frac{\partial\theta}{\partial t} = (-\dot{q}\frac{cos\chi}{\Delta} + \dot{\chi}\frac{(q-x)sin\chi + ycos\chi}{\Delta} - \frac{\dot{\Delta}}{\Delta}\frac{(x-q)cos\chi + ysin\chi}{\Delta})sin\theta \tag{14}$$

In Eq. 14, the term multiplying $\dot{\chi}$ may alternatively be written in the form below, simplifying calculations:

$$\frac{(q-x)sin\chi + ycos\chi}{\Delta} = \frac{y - \Delta sin\chi ln(tan(\theta/2))}{\Delta cos\chi} \tag{15}$$

Plugging in the ansatz into the Lagrangian and Dissipation density functions, integrating with respect to the x and y directions, and then plugging into the Euler-Lagrange equations, we get the following four equations of motion for the DW in terms of the collective coordinates:

$$\dot{\phi} + \alpha\frac{\dot{q}}{\Delta}cos\chi - \alpha\frac{\dot{\chi}}{cos\chi}\frac{w}{2\Delta} = \beta\frac{u}{\Delta}cos\chi + \mu_0\gamma\left[H_z + \frac{\pi}{2}\tau_{SL}\left(sin\phi u_{SOT,x} - cos\phi u_{SOT,y}\right)\right] \tag{16}$$

$$\begin{aligned}\frac{\dot{q}}{\Delta}cos\chi - \alpha\dot{\phi} - \frac{\dot{\chi}}{cos\chi}\frac{w}{2\Delta} =& \frac{\gamma}{M_s}K_s sin\left(2(\phi-\chi)\right) - \frac{\pi D\gamma}{2\Delta M_s}sin(\phi-\chi) + \frac{u}{\Delta}cos\chi \\ &+ \mu_0\gamma\frac{\pi}{2}\left[H_x sin\phi - H_y cos\phi\right] + \mu_0\gamma\tau_{SL}u_{SOT,z}\end{aligned} \tag{17}$$

$$\begin{aligned}\alpha\frac{\pi^2}{12}\left[\frac{\dot{\Delta}}{\Delta} - \frac{\dot{\chi}}{cos\chi}\right] =& \frac{\gamma}{M_2}\left[\frac{A}{\Delta^2}\left(1 + sin2\chi\right) - \left(K_u + K_s sin^2(\phi-\chi)\right)\right] \\ &+ \frac{\pi}{2}\mu_0\gamma\left(H_x cos\phi + H_y sin\phi\right)\end{aligned} \tag{18}$$

$$\alpha\frac{\pi^2}{12}\left[\frac{\dot{\Delta}}{\Delta}-\frac{\dot{\chi}}{cos\chi}\left(\left(\frac{w}{\pi\Delta}\right)^2+\frac{sin^2\chi}{2}\right)\right]=$$
$$\frac{\gamma}{M_s}\left[\frac{A}{\Delta^2}\left(2cos^3\chi+sin\chi\right)+sin\chi\left(K_u+K_ssin^2(\phi-\chi)\right)-cos\chi K_ssin\left(2\left(\phi-\chi\right)\right)\right] \quad (19)$$
$$+\frac{\pi D\gamma}{2\Delta M_s}sin\phi+\frac{\pi}{2}\mu_0\gamma sin\chi\left[H_xcos\phi+H_ysin\phi\right]$$

In the above equations, $u_{SOT,i}$ has been added to denote the direction of the spin-orbit interaction. They will be equal to 1 if spin orbit interactions exist in the i direction, and 0 otherwise. Note that w is the width of the sample, which enters calculations due to the inclusion of the y direction in the ansatz. Also note that, to simplify the above equations, the effective applied fields were introduced, defined as $H_i = H_{a,i} + \tau_{FL}u_{SOT,i}$ in which i denotes the directions x, y and z.

5 Field Driven DW Motion: Energy Landscape Comparison

It is known that 1-D model results may not quantitatively match those of micromagnetic simulations, while they have similar qualitative features. This could be attributed to constraints on the magnetization dynamics introduced by the use of the ansatz. In order to improve the quantitative predictive accuracy of the 1-D model, we hypothesize that the constraint torques may be identified by comparing energies or torques predicted by the 1-D model description to those from micromagnetics. These constraints could be added to the 1-D model as a correction. In this preliminary analysis, we look at the relationship between the difference in energy predictions from the two models and the collective coordinates used of the 1-D model.

In the derivation of the 1-D model, several energy terms are included in the Lagrangian.

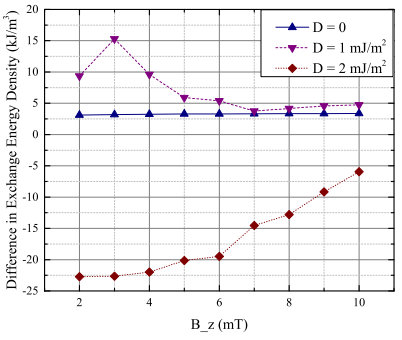

(a) Exchange energy.

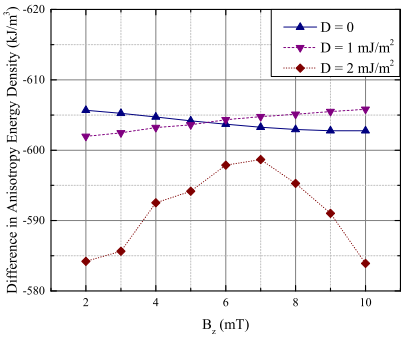

(b) Anisotropy energy.

Figure 3: Variation in the difference in the energies calculated from micromagnetic simulations compared to the 1-D model for (a) exchange energy, and (b) anisotropy energy.

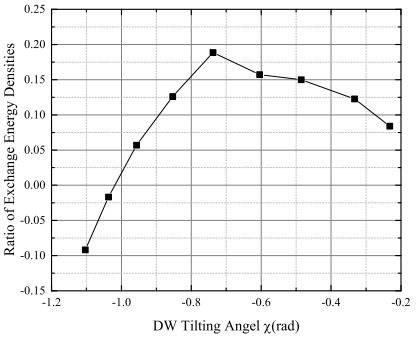

(a) Variation of exchange energy ratio with DW tilting angel χ.

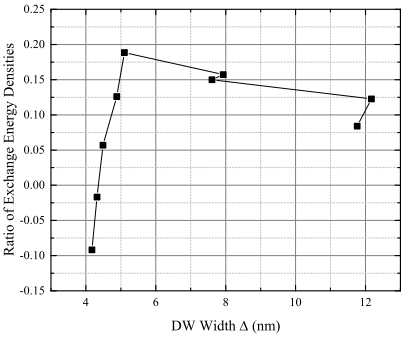

(b) Variation of exchange energy ratio with DW width Δ.

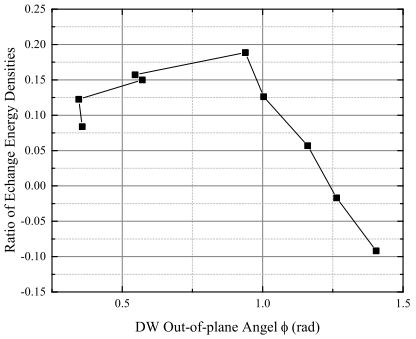

(c) Variation of exchange energy ratio with DW out-of-plane angel ϕ.

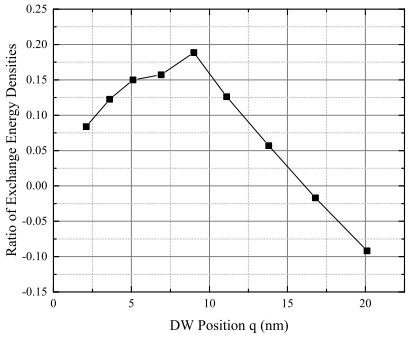

(d) Variation of exchange energy ratio with DW position q.

Figure 4: Variation of the difference in exchange energy calculated from micromagnetic simulations compared to the 1-D model with (a) the DW tilt angle (χ), and (b) DW width (Δ).

These energy terms are integrated in the x direction in order to remove spatial dependence and used to derive the four equations of motion listed in the previous section. The 1-D model exchange and DMI energy terms, when integrated on the length of the wire will take the following form:

$$E_{Exchange} = \int_{-\infty}^{\infty} A|\nabla m|^2 dx = \frac{2A}{\Delta}\left[\frac{1}{cos\chi} + 2sin\chi\right] \tag{20}$$

$$E_{DMI} = \int_{-\infty}^{\infty} D(m_z \nabla.\vec{m} - (\vec{m}.\nabla)m_z)dx = \frac{\pi D}{cos\chi} cos(\phi - \chi) \tag{21}$$

$$E_{Anisotropy} = \int_{-\infty}^{\infty} \left(K_U + K_s sin^2\left(\phi - \chi\right)\right) sin^2\theta dx = \frac{2\Delta}{cos\chi}\left(K_U + K_s sin^2(\phi - \chi)\right) \tag{22}$$

The energy densities in each case can be calculated by dividing the above equations by the length of the sample.

In order to assess the predictive accuracy of these energy terms, micromagnetic simulations were performed using the open source micromagnetic simulation environment mumax^3 [34]. Simulations were performed with the following material properties: $A = 10^{-11} J/m$, $M_s = 0.6 \times 10^6 A/m$, $K = 0 J/m^3$, $K0 = 0.59 \times 10^6 J/m^3$, and $\alpha = 0.02$. The sample was assumed to be $768nm \times 192nm \times 3nm$. The DMI strength was varied, $D = 0$, 1 and $2mJ/m^2$. Fields were applied in the z direction from 2 mT to 10 mT. mumax^3 can provide exchange and anisotropy energy as outputs, while also calculating the collective coordinates of interest to us. Note that the exchange energy output from Mumax^3 is the sum of exchange and DMI energies [34].

We used the final prediction of the collective coordinates by the mumax^3 simulation as the basis of energy calculations using the 1-D model analytical form of the energies (Eqs. 20 and 22 above). We would expect that the 1-D model and micromagnetic simulation predict energies that are nearly identical; however, this is not true as an energy difference exists, which could be attributed to the constraining torques introduced by the ansatz. Figure 3 outlines how the difference in the exchange and anisotropy energies varied with the applied field. Figure 4 illustrates the variation of the ratio of the exchange energy from mumax^3 to that of the 1-D model with the four collective coordinates for the case of D = 1 mJ/m^2. Δ and χ are the only coordinates that affect exchange energy according to Eq. 20; however, trends could be seen in the figure with DW position and, to an extent, with ϕ. Based on Figure 4, the energy ratios seem to follow strict functional forms which could be extracted as analytical corrections to the 1-D model. As an example, using regression analysis, the following equation could be used to describe the ratio of exchange energy at a DMI value of 0.001 J/m^2 in terms of the two collective coordinates which directly affect exchange energy according to the model, with an R^2 value of 0.9943:

$$E_{mumax}/E_{1-Dmodel} = a_0 + a_1\chi + a_2\Delta + a_3\chi^2 + a_4\Delta\chi \tag{23}$$

with $a_0 = -0.5785$, $a_1 = -2.367$, $a_2 = 3.769 \times 10^7$, $a_3 = -1.528$, and $a_4 = 9.207 \times 10^7$. The coefficients listed here are only valid for the specific case of D = 1 mJ/m^2, material properties noted above and the specific geometry studied. In fact, further studies are needed to understand the relationship between the coefficients in such energy difference functions and the input parameters of the simulation. However, overall, it seems that analytical descriptions of the constraint forces could be extracted on the basis of such energy analysis and added to the Lagrangian during the derivation of the 1-D model. This new Lagrangian will lead to additional corrective terms in the final description of the dynamics, improving the accuracy of the 1-D model. The comparison of the energy landscape of the two models may also help identify new coordinates or ansatz, leading to overall improvements of analytical modelling of DW motion.

6 Conclusion and Outlook

In this paper, we first derived the 1-D model for the motion of a tilting Bloch domain wall in perpendicularly magnetized ferromagnetic materials. We then showed preliminary results of how corrections could be developed by comparing the energy landscape of the 1-D model to that predicted from micromagnetic simulations.

We are now performing further studies to develop analytical functional forms for the corrective energy terms based on material properties and the collective coordinates in order to introduce additional terms in the 1-D model Lagrangian with the hope of improving the quantitative accuracy of this model.

Acknowledgments

This study was conducted as part of the Marie Currie ITN WALL project, which has received funding from the European Unions Seventh Framework Programme for research, technological development and demonstration under grant agreement no. 608031.

References

[1] S. Bader, S. Parkin, Spintronics, Annual Review of Condensed Matter Physics 1 (1) (2010) 71–88.

[2] C. H. Marrows, B. J. Hickey, New directions in spintronics, Phil. Trans. R. Soc. A 369 (1948) (2011) 3027–3036.

[3] H. Zabel, Progress in spintronics, Superlattices and Microstructures 46 (4) (2009) 541–553.

[4] H. Ohno, A window on the future of spintronics, Nature Materials 9 (2010) 952–954.

[5] G. Hrkac, J. Dean, D. A. Allwood, Nanowire spintronics for storage class memories and logic, Phil. Trans. R. Soc. A 369 (1948) (2011) 3214–3228.

[6] G. Catalan, J. Seidel, R. Ramesh, J. F. Scott, Domain wall nanoelectronics, Rev. Mod. Phys. 84 (2012) 119–156.

[7] R. L. Stamps, S. Breitkreutz, J. kerman, A. V. Chumak, Y. Otani, G. E. W. Bauer, J.-U. Thiele, M. Bowen, S. A. Majetich, M. Klui, I. L. Prejbeanu, B. Dieny, N. M. Dempsey, B. Hillebrands, The 2014 magnetism roadmap, J. Phys. D: Appl. Phys. 47 (33) (2014) 333001.

[8] D. A. Allwood, G. Xiong, C. C. Faulkner, D. Atkinson, D. Petit, R. P. Cowburn, Magnetic domain-wall logic, Science 309 (5741) (2005) 1688–1692.

[9] J. Jaworowicz, N. Vernier, J. Ferre, A. Maziewski, D. Stanescu, D. Ravelosona, A. S. Jacqueline, C. Chappert, B. Rodmacq, B. Dieny, Magnetic logic using nanowires with perpendicular anisotropy, Nanotechnology 20 (21) (2009) 215401.

[10] L. Thomas, M. Hayashi, R. Moriya, C. Rettner, S. Parkin, Topological repulsion between domain walls in magnetic nanowires leading to the formation of bound states, Nat. Commun. 3 (2012) 810–.

[11] S. P. Parkin, M. Hayashi, L. Thomas, Magnetic domain-wall racetrack memory, Science 320 (5873) (2008) 190–194.

[12] S. Parkin, S.-H. Yang, Memory on the racetrack, Nature Nanotechnology 10 (2015) 195?198.

[13] J. A. King, D. Eastwood, L. K. Bogart, H. Armstrong, M. Bath, D. Atkinson, Chiralmem: a novel concept for high density magnetic memory technology, in: Nanotech Conference and Expo 2009, 2009.

[14] J. Katine, E. E. Fullerton, Device implications of spin-transfer torques, J. Magn. Magn. Mat. 320 (7) (2008) 1217–1226.

[15] T. Gilbert, A phenomenological theory of damping in ferromagnetic materials, Magnetics, IEEE Transactions on 40 (6) (2004) 3443–3449.

[16] G. Tatara, H. Kohno, J. Shibata, Microscopic approach to current-driven domain wall dynamics, Physics Reports 468 (6) (2008) 213 – 301.

[17] A. Brataas, A. D. Kent, H. Ohno, Current-induced torques in magnetic materials, Nat Mater 11 (5) (2012) 372–381.

[18] S. Zhang, Z. Li, Roles of nonequilibrium conduction electrons on the magnetization dynamics of ferromagnets, Phys. Rev. Lett. 93 (12) (2004) 127204.

[19] A. Thiaville, Y. Nakatani, J. Miltat, Y. Suzuki, Micromagnetic understanding of current-driven domain wall motion in patterned nanowires, Europhys. Lett. 69 (2005) 990–996.

[20] M. I. Dyakonov, Spin Hall Effect, ArXiv e-prints.

[21] A. V. Khvalkovskiy, V. Cros, D. Apalkov, V. Nikitin, M. Krounbi, K. A. Zvezdin, A. Anane, J. Grollier, A. Fert, Matching domain-wall configuration and spin-orbit torques for efficient domain-wall motion, Phys. Rev. B 87 (2013) 020402.

[22] E. van der Bijl, R. A. Duine, Current-induced torques in textured rashba ferromagnets, Phys. Rev. B 86 (2012) 094406.

[23] K. Garello, I. M. Miron, C. O. Avci, F. Freimuth, Y. Mokrousov, S. Bluegel, S. Auffret, O. Boulle, G. Gaudin, P. Gambardella, Symmetry and magnitude of spin-orbit torques in ferromagnetic heterostructures, Nat. Nano. 8 (8) (2013) 587–593.

[24] A. Thiaville, S. Rohart, E. Jué, V. Cros, A. Fert, Dynamics of dzyaloshinskii domain walls in ultrathin magnetic films, EPL (Europhysics Letters) 100 (5) (2012) 57002.

[25] E. Martinez, L. Lopez-Diaz, O. Alejos, L. Torres, Resonant domain wall depinning induced by oscillating spin-polarized currents in thin ferromagnetic strips, Phys. Rev. B 77 (14) (2008) 144417.

[26] G. Tatara, E. Saitoh, M. Ichimura, H. Kohno, Domain-wall displacement triggered by an ac current below threshold, Applied Physics Letters 86 (23) (2005) –.

[27] R. A. Duine, A. S. N. nez, J. Sinova, A. H. MacDonald, Functional keldysh theory of spin torques, Phys. Rev. B 75 (21) (2007) 214420.

[28] E. Martinez, L. Lopez-Diaz, O. Alejos, L. Torres, C. Tristan, Thermal effects on domain wall depinning from a single notch, Phys. Rev. Lett. 98 (26) (2007) 267202.

[29] G. Consolo, E. Martinez, The effect of dry friction on domain wall dynamics: A micromagnetic study, J. Appl. Phys. 111 (7) (2012) –.

[30] O. Boulle, S. Rohart, L. D. Buda-Prejbeanu, E. Jué, I. M. Miron, S. Pizzini, J. Vogel, G. Gaudin, A. Thiaville, Domain wall tilting in the presence of the dzyaloshinskii-moriya interaction in out-of-plane magnetized magnetic nanotracks, Phys. Rev. Lett. 111 (2013) 217203.

[31] J. C. Slonczewski, Dynamics of magnetic domain walls, AIP Conference Proceedings 5 (1) (1972) 170–174.

[32] A. Thiaville, Y. Nakatani, Spin Dynamics in Confined Magnetic Structures III, Vol. Volume 101/2006 of Topics Appl. Phys., Springer, Berlin–Heidelberg, 2006, Ch. Domain-Wall Dynamics in Nanowires and Nanostrips, pp. 161–205.

[33] E. Martinez, S. Emori, N. Perez, L. Torres, G. S. D. Beach, Current-driven dynamics of dzyaloshinskii domain walls in the presence of in-plane fields: Full micromagnetic and one-dimensional analysis, Journal of Applied Physics 115 (21) (2014) –.

[34] A. Vansteenkiste, J. Leliaert, M. Dvornik, M. Helsen, F. Garcia-Sanchez, B. Van Waeyenberge, The design and verification of mumax3, AIP Advances 4 (10) (2014) –.